Surface roughness of Ti6Al4V samples produced by laser powder bed fusion for bone implants

M. Mhlanga, *L.R.* Masheane, *I.* Yadroitsava, & *I.* Yadroitsev

Department of Mechanical and Mechatronics Engineering, Central University of Technology, Free State, Bloemfontein, South Africa

Abstract. This study describes the surface roughness of heat-treated Ti6Al4V ELI samples without surface finishing (as-built condition) depending on the position of the build plate. Surface roughness was studied at the top and side surfaces of horizontal and vertical samples using a profilometer and Scanning Electron Microscopy. Morphology of tested samples is shown. It was shown that the top and side surfaces of vertical and horizontal samples had different morphologies, but they had fairly close roughness values, since the formation of roughness was mainly associated with sticking of the powder material both on the upper surface of the samples and on the side surfaces. It was found that samples that were far away from the argon inlet and recoater start line had higher surface roughness.

1 Introduction

Laser powder bed fusion (L-PBF) is a type of additive manufacturing (AM) where parts are produced directly from digital data. L-PBF technology has the capability to produce parts with high geometric complexity. L-PBF is AM technology where parts are produced with a laser beam selectively melting the powder layer by layer until the required product is formed [1]. AM has more advantage when compared to traditional manufacturing, such as less material waste and the ability to build objects with complex shapes [2], [3]. L-PBF can manufacture lattices and cellular structures, parts with complex internal features and objects with functional gradients. This technology has grown exponentially in many sectors such as biomedical, aerospace, and automotive and it still extending to other sectors [4]. However, the L-PBF still faces a challenge with product quality such as poor surface finishing. There are several peculiarities of the L-PBF process: layer by layer manufacturing causes staircase effect; the diameter of the laser spot, particle size distribution of powder, the features of powder layer deposition, manufacturing strategy, process parameters affect the porosity, mechanical and fatigue properties, as well as the roughness of L-PBF objects [5]. The high concentration of laser energy input leads to a high thermal gradient which induces residual stress within the as-built parts. High residual stress and specific anisotropic microstructure also require post heat treatment [7-9].
In general, the as-built L-PBF components have an irregular surface and high surface roughness is caused by several phenomena:

- Track-by-track, layer-by-layer nature of L-PBF manufacturing [8]-[9].
- The presence of unfused and attracted particles [9].
- The rippling effect that takes place in L-PBF, also influences the roughness of the top surface [3].
- The build orientation intrinsically generates a staircase effect. This depends on the inclination angle and layer thickness [3, 13].

Samples manufactured at similar process parameters but located at different areas of the base plate might have different mechanical properties and porosity as it was shown in [10] recently. The combined effect of the shaking and rolling during powder recoating leads to filtration of powder material (figure 1a): smaller powder particles remain near the start area of the recoating while bigger and medium particles move upwards and then, during recoating, to the opposite part of the build plate (see figure 1b). It was also shown that the re-coating process and gas flow effects on surface roughness of L-PBF samples inclined at different angles [11].

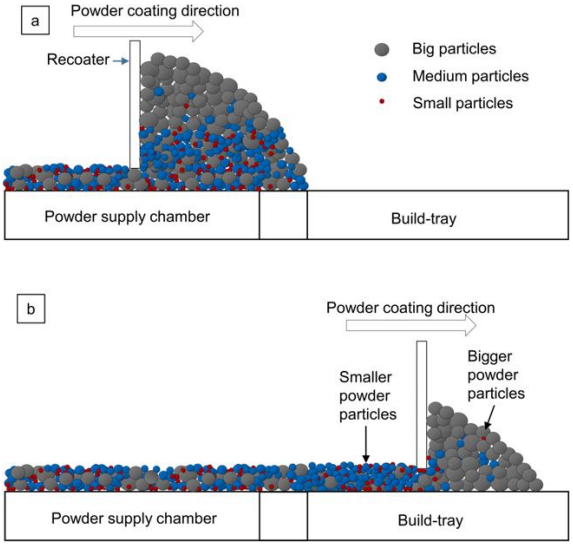

Figure 1: Powder flow and arrangement mechanisms during collecting and spreading them during the SLM process. The re-coater collecting the powder from the supply chamber (a) and the re-coater spreading the powder on the build tray (b) [10]**.**

Ti6Al4V is mostly used alloy to produce medical implants due to its attractive benefits such as good biocompatibility and corrosion resistance. Before a metal components may be placed into a body, many requirements must be met, one of this is a specific surface roughness [12].
According to ASTM F1378 standard, the metallic bearing surface of the shoulder prostheses shall have an average roughness (Ra) not higher than 0.10 μm (measured with a cut-off length of 0.25 mm) [13]. According to the ISO-7602-2 standard, the femoral head components of the total hip joint prosthesis the spherical articulating surfaces of metallic components shall have Ra maximum values not greater than 0.05 μm and a total height of the profile (Rt) maximum value not higher than 1.0 μm (measured using a cut-off value of 0.08 mm) and the maximum limit established for the internal surface of the hip joint acetabular cup is 2.0 μm. The femoral components of the metal knee prosthesis and the metal tibial articulating components of a mobile bearing knee shall have a Ra value less or equal to 0.1 μm (a cut-off value of 0.08 mm). According to ISO 7207-2 standard, a surface quality on the external surface of the knee prosthesis is specified with the arithmetic roughness such as 0.025μm<Ra<0.05μm. ISO 7207-2-2011 also states that when examined with normal or corrected vision, the articulating surface shall be free from embedded particles, defects and raised edges, scratches and score marks other than those arising from the finishing process [14]. The surface finish shall be uniform and free from marks that have been caused by previous operations, such as grinding, polishing, burnishing, tumbling, etc [15]. According to ISO 21536, for metallic components a surface roughness value Ra of 1.5 μm with a cut-off length of 0.8 mm is satisfactory for non-articulating regions that can be exposed to soft tissue [16]. The bone response is influenced by the implant surface condition: smooth Ra<0.5 μm and minimally rough (Ra 0.5-1 μm) surfaces showed less strong bone responses than rougher surfaces. Moderate rough (Ra 1-2 μm) surface demonstrate a stronger bone response compared to rough (Ra 2 μm). [17]. A

long-term keeping Ti6Al4V component in the human body leads to a reaction between human tissues and metal material that influences the healing and remodeling process of tissues. It was also shown that soft-tissue adhesion correlates with specific surface finishing of Ti6Al4V samples [18]. The high roughness of the L-PBF component results in a bone to implant interlocking and improves osseointegration [19], but according to Chan *et al*. [20], the high surface roughness demonstrates poor wear resistance that makes it difficult for some biomedical use.

To produce high-quality implants, it is necessary to analyze the properties of L-PBF components. This work represents an initial stage in the study of wear resistance of L-PBF Ti6Al4V ELI in as-built condition and after surface finishing procedures such as blasting, grinding, hand polishing, chemical and electro-chemical polishing. Before using surface finishing procedures and studying wear resistance of L-PBF Ti6Al4V, it was decided to analyze the surface roughness of manufactured samples since they might have different surface roughness and morphology depending on the position on the build plate.

2 Material and methods

Ti6Al4V (ELI) horizontal and vertical bars with a dimension of 20 mm x 20 mm x 5 mm and semi-spheres of 20 mm in diameter were produced by L-PBF with the EOSINT M290 system as recommended by EOS standard process parameters for Ti6Al4V ELI. All 45 samples were produced on one plate: 15 vertical bars, 15 horizontal bars and 15 semi-spheres (figure 2a). Samples were heat treated at 650℃ for 3 hours for stress relieving and then annealed at 940℃ for 2 hours in a vacuum furnace as stated in [1], figure 2a. Vertical bars in the future will be used to study surface finishing and wear resistance of side surfaces (wear resistance between layers) and horizontal ones will be used for surface finishing procedures and inter-track wear resistance (top surfaces) studies. Semi-spheres were manufactured to study surface finishing procedures for L-PBF surfaces with expressed stair-step effect.

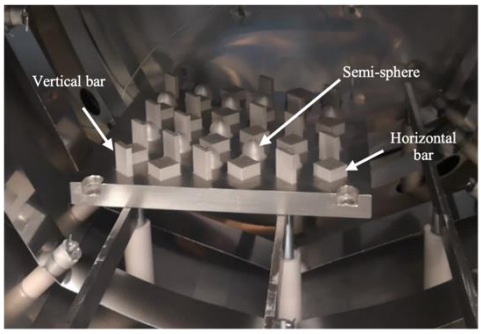

(a)

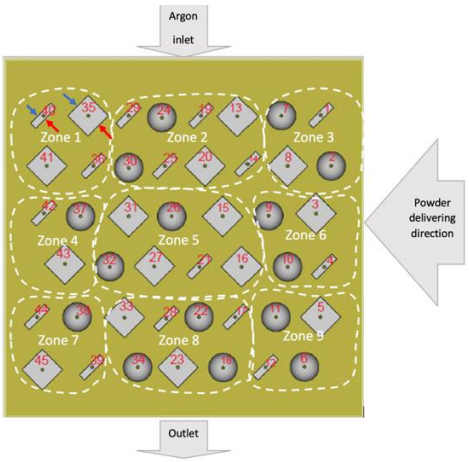

(b)

Figure 2: Plate with samples in a vacuum furnace (a) and (b) location of samples on the plate with indication of Ar feeding and powder delivering directions. Red arrows indicate side A, blue arrows indicate side B where surface roughness was analysed.

Before the measurement of surface roughness and microscope evaluation all the samples were submerged in the ultrasonic bath for 5 minutes in water. The horizontal and vertical bars samples were measured for surface roughness in the as-build condition which means no surface finishing has been done. Note that the surface roughness of the semi sphere samples was not measured in this work, only microscopic analysis was done. An average roughness (Ra), root means square (Rq) and ten-point height (Rz) were measured using Mitutoyo Surftest SJ-210 according to ISO 427:1997 with a cut of the length of 0.8 μm and evaluation length of 4 mm for a single measurement. Measurements were taken 3 times at randomly chosen areas on top and both side surfaces (A and B, figure 3b) of each sample. In horizontal samples, side surfaces were tested along layers, and in vertical samples, surface roughness was measured in a perpendicular direction, i.e., along the building direction. Samples were grouped and then analyzed by zones as shown in figure 2b with respect to Argon (Ar) blowing and powder delivering. So, samples from zones 1-3 were occurred near Ar inlet; the middle part consists of zones 4-6 and zones 7-9 were at the front of the build platform (near the gas outlet). Zones 3, 6 and 9 were near to start point of the recoater; zones 2, 5, and 8 were in the central part and zones 1, 4 and 7 were closer to the left side of the base plate. Measurements of each zones were averaged and t-test was done to compare average values of measured surface roughness. The JCM 5000 optical microscope was used to evaluate and validate both the side and top surface morphology of the horizontal, vertical, and semi-sphere samples.

3 Results and discussion

Average values and standard deviations of surface roughness for sides A and top surfaces are shown in figure 3. Measured profile roughness for side A was the highest in vertical sample #12 which occurred near the air outlet and closer to the powder delivering start area. The lowest value of surface roughness was in vertical sample #1 positioned near Ar inlet. For side B, maximum roughness was found for vertical sample #42 positioned on the opposite side from the powder delivering start area. Generally, average profile surface roughness was slightly higher for vertical samples. The reason is that vertical samples are heated for longer time, therefore adhering more powder particles. Also, horizontal and vertical samples were measured in different directions: perpendicular to building direction for horizontal samples and along it for vertical ones. The morphology of the side surface of the L-PBF samples is determined by the layered structure that might have valleys along the side of the scan track as well as attached powder particles on the

edges. The profilometer needle might slide along the layer and show lower value of surface roughness measured along the layer in comparison with the perpendicular direction.

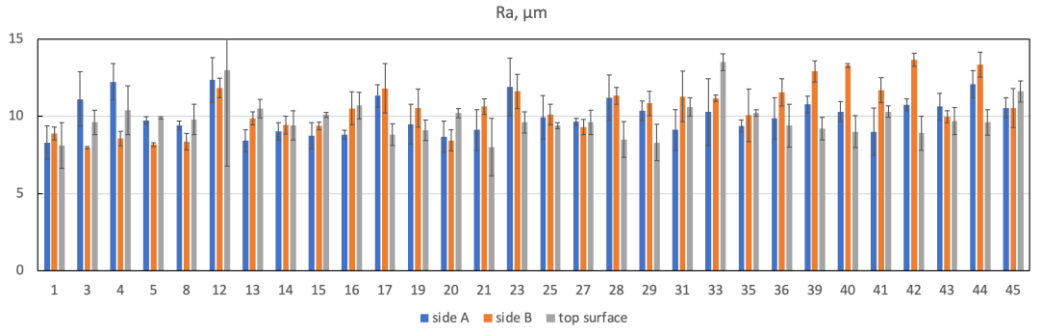

(a)

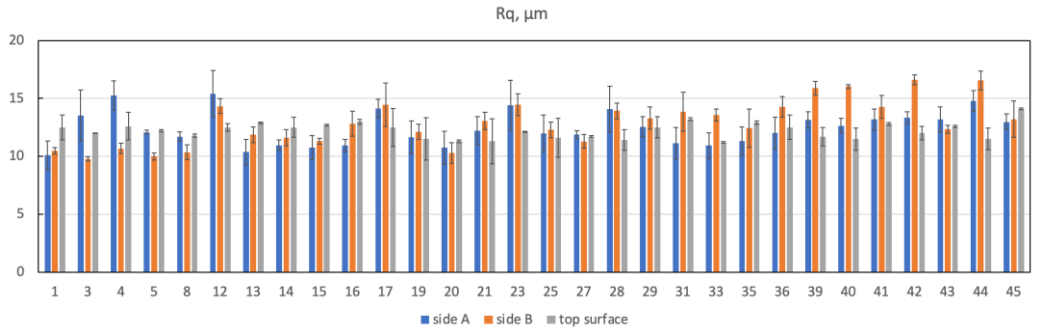

(b)

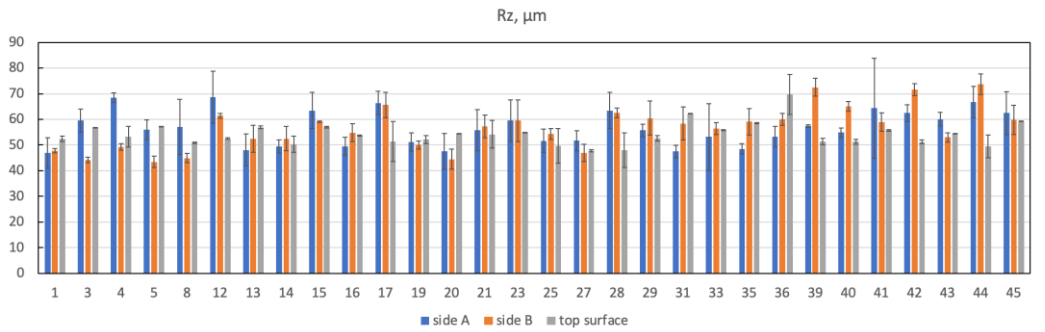

(c)

Figure 3: Surface roughness of tested samples: Ra (a), Rq (b) and Rz (c). A designation of samples is shown in figure 3.

So that our studies were not dependent on the direction of profile measurements, surface roughness was averaged for zones 1-9 considering all vertical and horizontal samples located in a certain area (see figure 2b). In zones situated on the opposite side of the plate from the start of powder spreading (zone #1) and in the middle (zone #5), the surface roughness Ra was higher at side B in comparison with side A, this difference was statistically significant (t-test, $p<0.05$), figure 5. At zones #4 and #7 Ra at side B varied significantly and showed a standard deviation of 2.05 and 1.55 µm that led to a statistically insignificant difference at chosen p-value (0.05). The opposite effect was found for surfaces located closer to the powder deposition started: side A had higher roughness at zone #6 ($p<0.05$) and zone 9. Zone #3 showed the lowest surface roughness measured by profilometer. A Ra roughness of top surfaces was 9-10 µm in average that correspond value received in [21]. Rz values were 50-70 µm, maximum was found in zone #7 (figure 4b). Minimum Rz was found at the top surface in samples from zone #3. A statistically significant difference

($p<0.05$) in average roughness Rz was found between Rz for the top surface at zone #3 and zones #1, 5, 6 and 9 where Rz was higher.

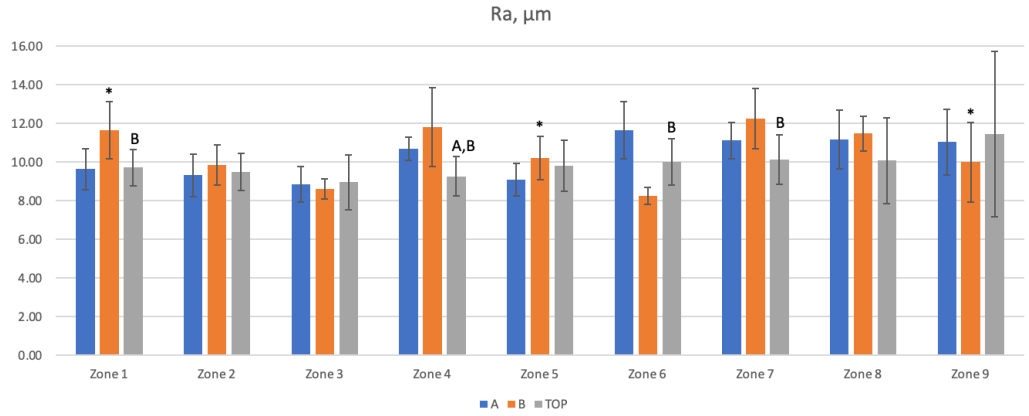

(a)

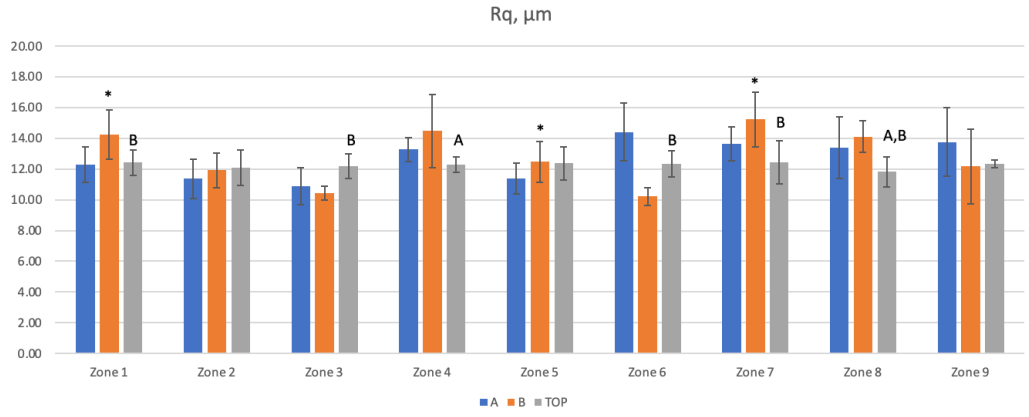

(b)

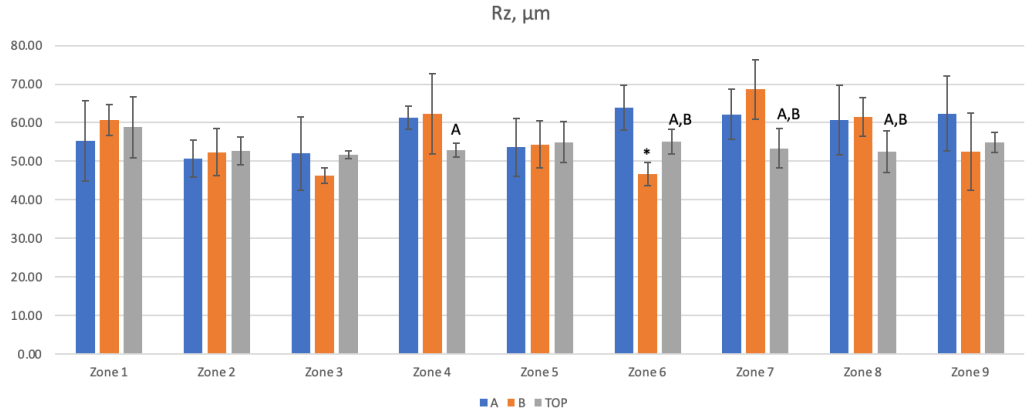

(c)

Figure 4: Surface roughness of tested samples: Ra (a), Rq (b) and Rz (c). A designation of zones is shown in figure 2; * shows statistically significant difference (t-test, $p<0.05$) between A and B sides from corresponding zone, A or B – in comparison side and top surface.

The high surface roughness on the side surface of the samples is a result of the adhered and partially melted powder particles as well as the morphology of the layer with the contouring track. Figure 5 shows the top view of the sample where the morphology of a single layer might be considered. A single layer consists of overlapped single tracks (core part) as well as a contouring track. Melt pool infiltrated powder particles, but adhered particles do not get enough time to melt; a high amount of them, due to rapid cooling as the scanning speed is high, are partially melted. A metallurgical bonding occurred between the vertical surface and adhered powder particles. During the melting of the powder by the laser, the powder particles that are closer to the literal boundary of the melt pool may attract toward the melt pool. The closer powder particle is either it melts completely or partly depend on the supplied energy density. As the melt pool solidifies, it causes the surrounding un-melted powder particles to adhere to the surface mostly on the side surface thereby increasing the roughness on the side surface. Spattering also inputs to surface roughness. The surface topography of the L-PBF sample is greatly affected by adhered partly melted powder particles and spatters onto the surface of the part [22]-[23].

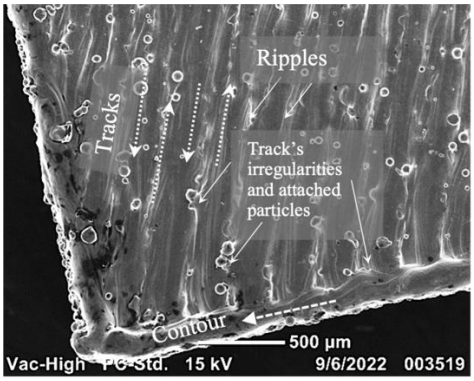

Figure 5: Top view of the L-PBF sample showing single layer morphology.

Figure 6 shows the side surface morphology of L-PBF samples. Morphology of the side surface is mainly due to attached powder particles that cover side surface as a coat. Since sample was manufactured with the contouring, the vertical surface looks quite smooth. SEM analysis of the morphology of samples revealed that the side of samples located near the start area of powder recoating had more residual attached fine particles (figure 6).

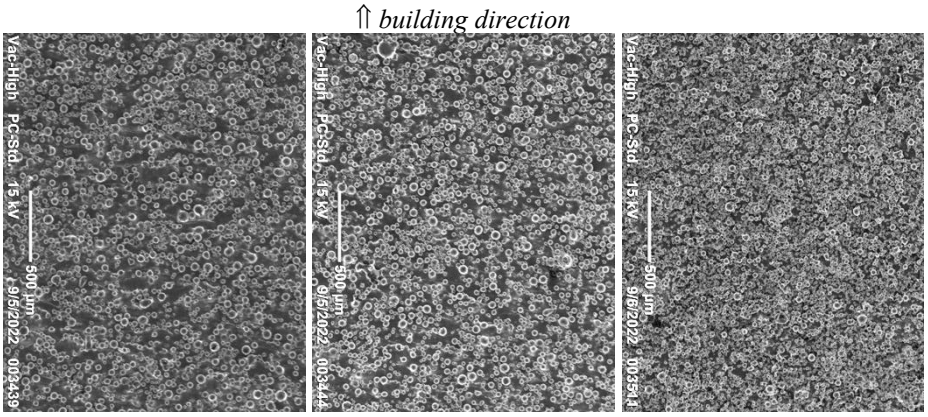

(a) (b) (c)

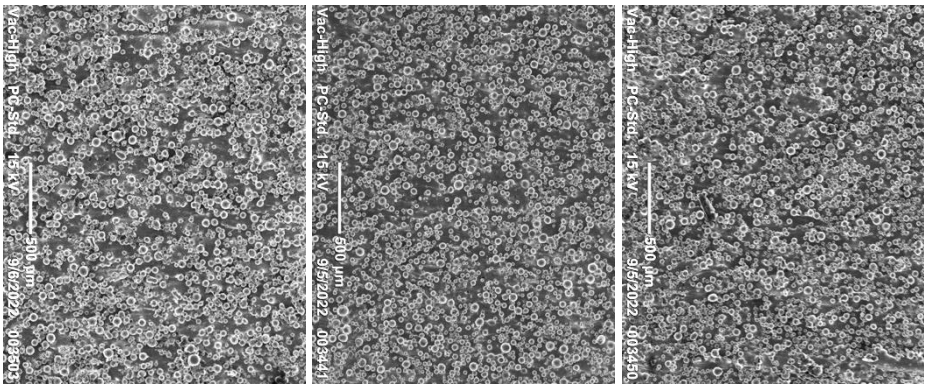

(d) (e) (f)

Figure 6: SEM photo of side surfaces A of vertical samples from zone #1 (a), #2 (b), #3 (c) and #7 (d), #8 (e), #9 (f).

The surface roughness at the top surface is caused by track-by-track formation, ripples formation and attached powder particles as shown in figures 5 and 7. Track-by-track manufacturing causes peaks and valleys that might form waviness on the top surface. Ripples on the track happen when the surface tension exerts a shear force on the liquid surface [23]. The surface roughness of the L-PBF is not only affected by powder particles that adhered to the surface due to elevated local temperature and spattering, but the ripples also influence the roughness of the top surface. According to Simson [23], the fluid convection in the melt pool is the primary reason for the position of the adhered powder particles and thermocapillary convection and unsteady deformation of the free surface near the solidification front appears is responsible for the formation of rippling. The powder particles adhered to the surface during solidification and ripples does contribute to the roughness of the top surface of the L-PBF parts. Figure 7 shows the top surfaces morphology of Ti6Al4V samples, there are many droplets of partially melted powder particleson the top surface. Even though the partly powder particle adhered to the surfaces is reduced at the top surface in comparison with side surfaces, the surface roughness of the as-built samples is still high (figure 5). The surface roughness of L-PBF Ti6Al4V ELI is too high compared to what is required by the implants as stated by ASTM and ISO standards.

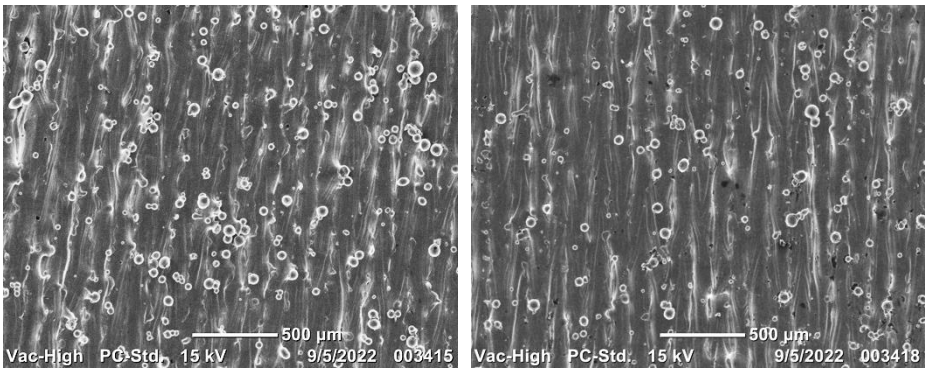

(a) (b)

Figure 7: SEM photo of top surfaces of horizontal samples from zone #1 (a) and zone #3 (b).

L-PBF builds parts layer by layer, for inclined parts the layers are forming a staircase. These stairs also contribute to the surface irregularities of the L-PBF part [5], [18]. Figure 8 shows the staircases and partially melted powder particles adhered to the surface of the semi-sphere sample.

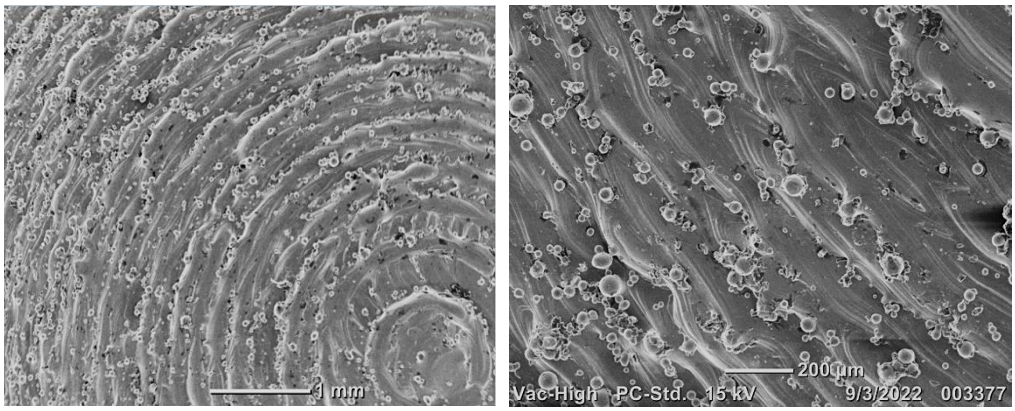

(a) (b)

Figure 8: Surface morphology of the semi sphere sample at different magnifications.

Since the morphology of surfaces was mainly determined by attached powder particles, values of surface roughness for sides and top surface averaged by all measurements were close to each other (see figure 9): Ra was about 10 µm, Rq was near 12 µm and Rz was about 54-57 µm. But the topology of surfaces was different: side surfaces were tightly coated by powder particles while top surfaces consisted of overlapped quite irregular tracks with attached powder particles. Thus, wear tests of as-built surfaces and post-processing such as surface finishing might also lead to different surface morphology that will be done in the next study.

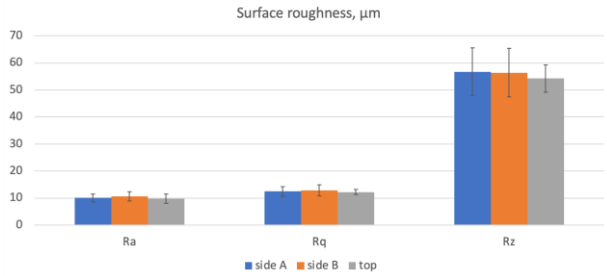

Figure 9: Averaged roughness of side A, B and top surfaces.

4. Conclusion

The values of side surface roughness were found to be compatible when compared with the top surfaces of vertical and horizontal samples. It was found that the location of the sample on the build plate has an effect on the roughness values and surface morphology. The samples that were far from argon inlet and re-coater start line had slightly higher roughness compared to samples that are closer to that. It is also clear as-built L-PBF surfaces are too rough and don't to meet the requirements of ISO and ASTM standards for metal implants. Therefore, surface finishing procedures will be done in future and the next step of the study is an analysis of post-processing of manufactured L-PBF samples for appropriate surface finishing for bone replacements.

Acknowledgements

A special word of appreciation to the South African Research Chairs Initiative of the Department of Science and Innovation and the National Research Foundation of South Africa (Grant № 97994) and the Collaborative Program in Additive Manufacturing (Contract № CSIR-NLC-CPAM-15-MOA-CUT-01) for the financial aid received for financial support and CRPM for manufacturing parts.

References

[1] I. Yadroitsev, P. Krakhmalev, and I. Yadroitsava, Selective laser melting of Ti6Al4V alloy for biomedical applications: Temperature monitoring and microstructural evolution, **583**, 404–409 (2014)
[2] J. V. Gordon, Defect structure process maps for laser powder bed fusion additive manufacturing, **36**, 101-552 (2020)
[3] H. Lee, C. H. J. Lim, M. J. Low, N. Tham, V. M. Murukeshan, and Y. J. Kim, Lasers in additive manufacturing, **4**, 307–322 (2017)
[4] M. A. Obeidi, Results in Engineering Metal additive manufacturing by laser-powder bed fusion : Guidelines for process optimisation, **15** (2022)
[5] M. Shange, I. Yadroitsava, S. Pityana, I. Yadroitsev, and D. Bester, Surface morphology characterisation for parts produced by the high speed selective laser melting, **655**, (2019)
[6] S. J. Davies, S. P. Jeffs, M. P. Coleman, and R. J. Lancaster, Effects of heat treatment on microstructure and creep properties of a laser powder bed fused nickel superalloy, **159**, 39–46 (2018)
[7] I. van Zyl, I. Yadroitsava, and I. Yadroitsev, Residual stress in TI6AL4V objects produced by direct metal laser sintering, **27**, 134–141 (2016)
[8] A. P. Nagalingam, M. S. Vohra, P. Kapur, and S. H. Yeo, Effect of cut-off, evaluation length, and measurement area in profile and areal surface texture characterization of as-built metal additive manufactured components, **11**, (2021)
[9] E. Masiagutova, F. Cabanettes, A. Sova, M. Cici, G. Bidron, and P. Bertrand, Side surface topography generation during laser powder bed fusion of AlSi10Mg, **47** (2021)
[10] S. Pal The effects of locations on the build tray on the quality of specimens in powder bed additive manufacturing, **112**, 1159–1170 (2021)
[11] Z. Chen, X. Wu, D. Tomus, and C. H. J. Davies, Surface roughness of Selective Laser Melted Ti-6Al-4V alloy components, **21**,91–103 (2018)
[12] N. M. HuangAnalyzing the Surface Finish of Knee Implants to Determine Criteria for Applications in Direct Metal Laser Sintering, (2012)
[13] S. Mat, Shoulder Prostheses , 1–6, (2004)
[14] ISO 17757, INTERNATIONAL STANDARD iTeh STANDARD iTeh STANDARD PREVIEW, *Int. Organ. Stand*, **10406**–1:20, 3–6 2019.
[15] S. Standard, "iTeh STANDARD PREVIEW iTeh STANDARD PREVIEW," **1** 2–5 (2020)
[16] DRAFT INTERNATIONAL STANDARD ISO / DIS 21535 Non-active surgical implants — Joint replacement implants — Specific requirements for hip-joint replacement implants ISO / CEN PARALLEL PROCESSING, (2021)
[17] A. Wennerberg and T. Albrektsson, Effects of titanium surface topography on bone integration: A systematic review,, **20**,172–184 (2009)
[18] M. I. Z. Ridzwan, S. Shuib, A. Y. Hassan, A. A. Shokri, and M. N. Mohammad Ibrahim, Problem of stress shielding and improvement to the hip implant designs, *Journal of Medical Sciences,***7**, 460–467, (2007)
[19] A. Barfeie, J. Wilson, and J. Rees, Implant surface characteristics and their effect on osseointegration, **218** (2015)
[20] D. Rodriguez, F. J. Gil, J. M. Manero, J. A. Planell, C. Fonseca, and M. Barbosa, Improvement of hardness and wear resistance of titanium and Ti6Al4V by nitrogen diffusion, **2,** 908–913 (1999)
[21] I. Yadroitsev, A. Du Plessis, and I. Yadroitsava, Basics of laser powder bed fusion, *Fundamental Laser Powder Bed Fusion Met*, 15–38 (2021)
[22] S. Pal , As-fabricated surface morphologies of Ti-6Al-4V samples fabricated by different laser processing parameters in selective laser melting, **33** (2020)
[23] D. Simson and S. K. Subbu, Effect of Process Parameters on Surface Integrity of LPBF Ti6Al4V, *Procedia CIRP*, **108,** 716–721, (2022)